Full Paper

www.molinf.com

molecular informatics

DOI: 10.1002/minf.202000096

Insights on 3D Structures of Potential Drug-targeting Proteins of SARS-CoV-2: Application of Cavity Search and Molecular Docking

Mariana S. Fernandes,[a] Francielly S. da Silva,[a] Ana Carolina S. G. Freitas,[a] Eduardo B. de Melo,[b] Gustavo H. G. Trossini,[c] and Fávero R. Paula*[a]

Abstract: The emergence of the COVID-19 has caused public health problems worldwide and there is no effective pharmacological treatment for this disease. Research on 3D models of proteins and the search for active molecular sites are important tools to assist in the discovery of effective antiviral drugs to combat COVID-19. To address this problem, the 3D protein structures of SARS-CoV 2 were analyzed and submitted to cavities research, evaluation of their druggabillity and liganbility, and applied to molecular docking studies with potential ligand candidates actually assayed against COVID-19. Eight druggable potential cavity sites were determined in model structures' PDB code, 6W4B, 6VWW, 6W01, 6M3M, and 6VYO, and these are the good alternatives to be characterized as targets for antiviral compounds. The good cavity model of the protease 3D structure was used in molecular docking, and this allowed verifying the theoric interactions of this protein and lopinavir and ritonavir antiviral drugs. These results may assist in the use of 3D protein models in drug design studies aiming to develop drugs against the COVID-19 pandemic.

Keywords: SARS-CoV-2 · COVID19 · 3D Structures · Cavity Search · Molecular Docking

1 Introduction

Coronaviruses are enveloped viruses with single RNA and their subtypes are distributed among humans, birds, and other mammals, and they are known to cause veterinary and human health diseases.[1] These viruses cause respiratory, enteric, liver, and neurological damage.[2,3] Seven coronaviruses have been recognized to cause diseases in humans. Four of them (229E, OC43, NL63 and HKU1) are prevalent and generally cause mild symptoms such as colds in immunocompetent individuals.[4] By 2018, two other strains were associated with fatal diseases: the coronavirus of the Middle East respiratory syndrome (MERS-CoV) and the coronavirus of the severe acute respiratory syndrome (SARS-CoV), both of zoonotic origin.[1] MERS-CoV was the agent responsible for severe outbreaks of respiratory diseases in the Middle East in 2012.[5] SARS-CoV was the causative pathogen of the severe outbreaks of acute respiratory syndrome in 2002 and 2003 in Guangdong province, China.[6–8]

In late December 2019, several health institutions in Wuhan, Hubei province, China, reported groups of patients with pneumonia of an unknown cause. These patients were epidemiologically linked to a seafood market.[9] The RNA collected from the patients allowed the isolation and identification of the sequence of a genome from a new coronavirus type, which was named 2019-nCoV.[10] The disease caused by this new variant of coronavirus, named COVID-19, is highly infectious and dangerous for vulnerable portions of the exposed population, such as diabetics, cardiac patients, and the elderly with respiratory and chronic diseases.[10,11] After the virus had been detected in 125 countries, the WHO declared COVID-19 a pandemic on 11 March 2020.[12]

Clinical research with COVID-19 indicates the occurrence of dyspnea and pneumonia,[11] which can occur on the fifth day, and an acute respiratory distress syndrome on the eighth day after the first symptom of COVID-19 in most patients infected. Other effects such as organ dysfunction and death can occur in severe cases.[11,13] Approximately 30,000 patients worldwide were confirmed to have died from the virus by the end of March, 2020. Emerging and reemerging pathogens are global challenges for public health, especially those that do not yet have an established treatment.[14] The research and discovery of bioactive compounds or repurposing drugs that can combat COVID-

[a] *M. S. Fernandes, F. S. da Silva, A. C. S. G. Freitas, F. R. Paula*
Course of Pharmacy, Federal University of Pampa (UNIPAMPA). BR 472, km 592, P.O. Box 118, 97500-970, Uruguaiana-RS, Brazil
phone/fax: +55 55 3413–4321
E-mail: faveropaula@unipampa.edu.br
[b] *E. B. de Melo*
Department of Pharmacy, State University of West Paraná (UNIOESTE). Universitária Street 2069, 85819-110, Cascavel-PR, Brazil.
[c] *G. H. G. Trossini*
Department of Pharmacy, University of São Paulo (USP). Lineu Prestes Avenue 580, 05508-900, São Paulo-SP, Brazil.

19 or even assist in its treatment are a priority for health institutions.

Currently, some therapeutic approaches have been suggested for use in treatment of infections caused by this virus, such as lopinavir-ritonavir, favipiravir, chloroquine, hydroxychroloquine, etc. Among these, the two viral protease inhibitors, lopinavir-ritonavir association, indicated as anti-HIV, have been indicated to have an antiviral effect against two coronaviruses, SARS and MERS.[15–18]

Another antiviral, remdesvir, was evaluated in the USA and also in China in patients who had developed severe problems from COVID-19 infection.[13,19] In the study carried out in China, this drug was used in conjunction with chloroquine, and it effectively inhibited the new coronavirus in "in vitro" trials. Another derivative of chloroquine, hydroxychloroquine, has also been studied by researchers where it presented good results "in vitro", and they recommended its insertion in studies in vivo. The derivatives of quinolines affect changes in intracellular pH, which can prevent the virus from proliferating in the human body.[20]

3D computational models of different molecular structures of SARS-CoV-2 have been carried out, and these are available in databases such as the Protein Data Bank.[21] The study of these structural models can be used to understand potential activity on viruses and also to design and develop new therapeutic agents.

A molecular modeling study published by Lin et al. (2020) evaluated models of viral protease and C30 coronavirus endopeptidase, together with a papain like viral protease (PLVP), and suggested a homology model of SARS-CoV-2 proteases.[22] In this work, molecular interactions between bioactive compounds and the 3D model protein may indicate the mechanism of action of these compounds in the virus multiplication cycle. Other research using the main virus protease crystal structures and the molecular docking and virtual screening tools provide basis for design compounds that are candidate to inhibit this viral protein.[23,24]

The present work aims to give some insights about the 3D molecular structures from SARS-CoV-2 and also determine computational structural information that allows researchers to analyze and identify potentially active sites and their druggabiity, which may be used for drug design. The computational strategies of cavity research of relevant proteins and the molecular docking between the virus proteins and the antiviral compounds ritonavir, lopinavir, remdesivir, and favipiravir were also performed aiming to understand the potential protein interactions and also to assist in the development of a treatment for the new coronavirus.

2 Experimental

2.1 Molecular Modelling

The computer program Spartan for Windows (version 08, Wavefunction, Inc., USA) was used for the design, and also to optimize molecular geometry and performing the conformational analysis using a systematic search, with torsion angle increases set to 30° in the range 0–360°, of the structure of antivirals ritonavir, lopinavir, remdesivir, favipiravir, and balaxovir marboxil. Calculations were performed using the semi-empirical methods AM1 followed by the empirical density functional theory (DFT) B3LYP using the theoretical database 6-31G*. At this stage, chemical structures of antiviral drugs with an optimized chemical structure were saved in PDB format prior to use in docking analysis.

2.2 Cavity Search

CavityPlus webserver software was used to identify cavities and connection sites, to predict the identification of allosteric sites and also the possibility of covalent ligand-binding occurrence, and to generate some pharmacophore measurements.[25] As the first step, the 3D protein models were downloaded using PDB code. The amino acid residues that constitute the molecular structure of the cavities will be identified in this step. In cavity search the following parameters were used: separated min depth, 8 Å; max abstract limit, 1.500 A^3; separate max limit, 6.000 A^3; min abstract depth, 2 Å; limit of the minimum value, 100 A^3; limit of the minimum score, 1.5. In this case, the software uses data of maximal experimental binding affinity with the PDBBind data set to predict cavity score (Pred Max pKd), the pKdAve that is the average binding affinity of the associated pocket, and a drugscore. CAVITY outputs were used for next steps such as the search of pharmacophore measurements, identification of allosteric and potential covalent interactions using CavPharmer, CorrSite, and CovCys applications. CavPharmer derives pharmacophore features such as a hydrophobic center, hydrogen bond donor and acceptor, positive and negative central points, and excludes volume. This software was applied only to improve the better druggable cavity generated by cavity search. CorrSite allows identification of the location of allosteric sites, and CovCys was used for the analysis of covalently modified cysteines. Both tools were used in results to find a 3D protein pocket with higher druggability.

2.3 Molecular Docking

The molecular docking analysis involved studies on the interaction between antivirals and the viral protease and replicase. The SARS-CoV-2 3D structures were downloaded

from PDB 6W63 (protease), 6W4B (replicase) and 6VWW (endoribonuclease) and submitted to treatment by removal of water molecules and the addition of polar hydrogens using the Autodock Tools 1.5.6.[26] At this stage, chemical structures of antiviral drugs with an optimized chemical structure were imputed in iGemdock 2.1 docking software (BioXGEM, TW).[27] These studies were performed in order to calculate the individual connections that the antivirals pose to docking in the viral proteins. These calculations were performed using parameters of genetic algorithm (GA) chosen for population size, generation, and number of solutions such as 400, 70 and 8, respectively, under application of a custom docking calculation. A range of five to ten Angstroms was studied in a grid (interaction box) cavity. The default functions of hydrophobic and electrostatic Gemdock scores (preference 1:1) were used in these calculations.

3 Results and Discussion

3.1 Chemical 3D Structures

By the end of March, approximately fifty-four 3D structures were found in the Protein Data Bank.[21] They involved models of protease, replicase, endoribonuclease, nucleocapsid-associated proteins, HR2 domain and glycoprotein, ADP phosphatase, and others. These structures and their characteristics are described in Table 1. In the course of time, several new structures of the SARS-CoV-2 virus and of the H1N1 virus should be submitted to this database according to development of new studies. The differences between these involve functions, the number of amino acid residues, the presence of subunits or chains, the absence and presence of complexes between ligands and protein, different conformations, and APO form or not. The study of these proteins can assist in understanding COVID-19 development and also in the design of active compounds that are candidates for antiviral drugs against SARS-CoV-2. Among the available structures, viral protease models are the principal number of 3D structures, and therefore they are presented as the main proposal for use in studies to predict therapeutic targets. The molecular structure of a 3D protease model (code PDB 6LU7)[28] is shown in Figure 1.

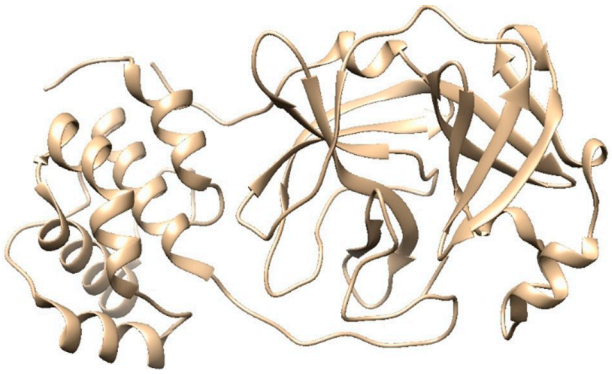

Figure 1. Molecular structure of protease code PDB 6LU7.[28] Graphic visualization obtained using USCF Chimera (v.1.10.1).

3.2 Cavity Search

Druggability is the probability that a biological protein be a good target, interact, and be modulated by a bioactive molecule inducing a biochemical effect resulting in a pharmacological activity. This property can be determined experimentally or predicted.[29] This is essential in the process of drug discovery and development. One of the methods to evaluate druggability is to perform a search for cavities or binding sites in proteins or cellular structures from a potential molecular target.[25] These cavities are potential regions for interaction with molecules which results in a pharmacological effect.

The software Cavity Plus implements a geometry-based method for ligand pocket site detection and analysis, and it allows the determination of a Cavity Score and Drug Scores that are used to quantitatively calculate the ligandability and druggability of a molecular binding site. The ligandability value represents the possibility of ligands interacting with a cavity. The score is influenced by cavity volume, pocket lip size, hydrophobic volume, cavity surface area, and hydrogen-bond-forming surface area.[25]

The possibility of druggable cavity occurrences in 3D protein structures of SARS-CoV-2 were studied using Cavity Plus webserver software, which aimed to discover potential molecular sites that may be used in virus inhibition. Some virus proteins such as replicases, proteases, and structural portions from the nucleocapsid are involved in the fusion of the virus (S2 subunit), a spike glycoprotein. Elucidated 3D structures available on the PDB database, in isolation or complexed with ligands, were submitted to cavity search studies for the purpose of assisting in the development of new drugs. The main results are shown below.

3.2.1 Replicase

The replicase, also known as RNA-dependent RNA polymerase, was available in the PDB database in March 2020.[30] The inhibition of this enzyme class has been suggested as a biological antiviral target for drugs such as remdesivir against Ebola and Marburg viruses,[31] MERS, and SARS-COV,[32] and favipiravir for influenza and West Nile virus.[33] These drugs have been suggested as potential treatments for COVID-19, and therefore these molecules may be acting on this SARS-CoV-2 protein.[34]

The 3D protein model may be used to search candidates for therapeutic targets. In this study, the PDB 6W4B model for Nsp9 replicase[30] was downloaded and submitted to a

Table 1. PDB database codes and 3D characteristics of SARS-CoV-2 proteins.

PDB Code	Date Deposit	Structure Function	Chain	Length Sequence
5R80	03/03/2020	Protease	A	306
5R81	03/03/2020	Protease	A	306
5R82	03/03/2020	Protease	A	306
5R83	03/03/2020	Protease	A	306
5R84	03/03/2020	Protease	A	306
5RE4	03/15/2020	Protease	A	306
5RE5	03/15/2020	Protease	A	306
5RE6	03/15/2020	Protease	A	306
5RE7	03/15/202	Protease	A	306
5RE8	03/15/2020	Protease	A	306
5RE9	03/15/2020	Protease	A	306
5REA	03/15/2020	Protease	A	306
5REB	03/15/2020	Protease	A	306
5REC	03/15/2020	Protease	A	306
5RED	03/15/2020	Protease	A	306
5REE	03/15/2020	Protease	A	306
5REF	03/15/2020	Protease	A	306
5REG	03/15/2020	Protease	A	306
5REH	03/15/2020	Protease	A	306
5REI	03/15/2020	Protease	A	306
5REJ	03/15/2020	Protease	A	306
5REK	03/15/2020	Protease	A	306
5REL	03/15/2020	Protease	A	306
5REM	03/15/2020	Protease	A	306
5REH	03/15/2020	Protease	A	306
5REN	03/15/2020	Protease	A	306
5REO	03/15/2020	Protease	A	306
5REP	03/15/2020	Protease	A	306
5RER	03/15/2020	Protease	A	306
5RES	03/15/2020	Protease	A	306
5RET	03/15/2020	Protease	A	306
5REU	03/15/2020	Protease	A	306
5REV	03/15/2020	Protease	A	306
5REW	03/15/2020	Protease	A	306
5REX	03/15/2020	Protease	A	306
5REY	03/15/2020	Protease	A	306
5REZ	03/15/2020	Protease	A	306
5RFO	03/15/2020	Protease	A	306
5RF1	03/15/2020	Protease	A	306
5R7Y	03/03/2020	Protease	A	306
6LU7	01/26/2020	Protease	A, C	312
6M03	02/19/2020	Protease	A	306
6Y37	03/25/2020	Protease	A	306
6Y84	03/03/2020	Protease	A	306
6LXT	02/11/2020	S2 Subunit	A, B, C, D, E, F	132
6LVN	02/04/2020	Viral protein	A, B, C, D	36
6VWW	02/20/2020	Endoribonucleasee	A, B	371
6W01	02/28/2020	Endoribonuclease	A, B	371
6W02	02/28/2020	ADP ribose phosphatase	A, B	173
6VSB	02/10/2020	Viral protein	A, B, C	1288
6VYO	02/27/2020	RNA binding domain of nucleocapsid protein	A, B, C, D	128
6W4B	03/10/2020	Replication viral protein	A, B	117
6M17	02/24/2020	Membrane protein/ viral protein	A, C	654
			B, D	814
			E, F	223
			E, F	
6VW1	02/18/2020	Cell invasion	A, B	597
			E, F	217

search for druggable cavities. Ten cavities were identified in this protein. Of these, one was druggable and two less druggable. The proposed cavity occurred at the junction of chain A and B, and it was considered to be better than others that are less druggable, since this cavity showed values of Prediction Maximum pkd (indicating the ligandability of cavity binding site) of 10.88 and druggability of 1075.00. The cavity from the 3D model is shown on the purple surface in Figure 2. All of the results predicted from

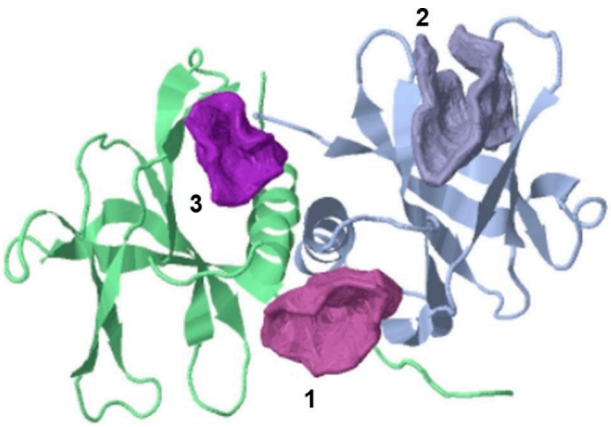

Figure 2. Molecular model 3D of Nsp9 replicase (PDB code 6W4B)[30] and cavities 1–3 in spatial regions using CavityPlus Software.

this protein are demonstrated in Table 2. The suggested amino acid residues from this cavity are expressed in Table 3.

3.2.2 Protease

The viral proteases encoded by genetic material have the function of catalyzing the hydrolysis of polyproteins in smaller portions that will assist the viral cycle and also the infectivity to biological cells.[35] Proteases have been used as targets for inhibitory drugs such as darunavir to fight HIV that causes AIDS,[36] and simeprevir is used against HCV in a treatment of hepatitis C. A hydrolase 3CL, called the main protease in SARS-CoV-2,[37] has been widely studied for drug discovery purposes, and this protein has more than 45 3D structural models deposited in the PDB database. The drugs loprinavir and ritonavir have been studied against SARS-CoV-2 and have been presented as alternatives for the treatment of COVID-19. This hypothesis however has been in doubt, because no significant clinical improvement was determined in trial studies.[38] Additionally, the literature comments that the HIV protease is an aspartic protease type and SARS-CoV belongs to cysteine protease families. Moreover, the HIV inhibitors were developed to interact with the C2 region of the catalytic site, and this site is absent in the SARS-CoV-2 protein.[39] In spite of these issues these authors suggest the antivirals' effects against the SARS-CoV-2 may reduce the time of patients in an ICU unit. Also, a feasible understanding about indirect interactions with this protease remains to be achieved.

Studies of cavities using the main protease of the virus that caused COVID-19 covered thirteen 3D models of the forty-five observed in the PDB database, including the ligand compound co-crystallized. The better protein evaluated was the PDB code 6W63 model with a chain A.[40] It was deposited in March 2020. In this prediction, a molecular cavity considered less druggable was determined. It showed a value to Pred. Max pkd of 11.26 and DrugScore 199.00. The amino acid residues located in the cavity were as follows: GLY 23, THR 24, THR 25, THR 26, LEU 27, ASN 28, HIS 41, VAL 42, ILE 43, CYS 44, THR 45, SER 46, GLU 47, ASP 48, MET 49, LEU 50, PRO 52, TYR 54, PHE 140, LEU 141, ASN 142, GLY 143, SER 144, CYS 145, HIS 163, SER 164, MET 165, GLU 166, LEU 167, PRO 168, THR 169, GLY 170, VAL 171, HIS 172, ALA 173, PHE 181, VAL 186, ASP 187, ARG 188, GLN 189, THR 190, ALA 191, and GLN192. Once the presence of ligand X77-A401 complexed with the protein was evaluated, it was verified that the same cavity without the presence of the ligand was obtained, and the results were the same in the two conditions evaluated.

The next protease model was PDB code 6LU7.[28] It is coupled with the N3 linker and contains structural chains A and C with 306 and 6 amino acid residues, respectively. It was found that the results obtained allowed the determination of 10 cavities considered to be undruggable. Once the chain A was evaluated individually, a cavity considered less druggable was predicted, however its value was negative. The C subunit model has a much-reduced molecular structure and this did not allow it to be correctly evaluated.

Another PDB model, code 5R80, with an A subunit only, complexed to compound Z18197050 in its structure.[41] It was submitted to a cavity search, and it showed ten molecular sites considered to be undruggable, demonstrating all negative drugscore values. The main protease models obtained by the authors from PanDDA analysis (5R7Y, 5R7Z, 5R83, and 6M03),[42–45] which correspond to protease in apo form, were also submitted to cavity analysis and none of them resulted in the observation of cavities considered useful, since they were undruggable. Thus, these models, which did not present any druggable site, are not the main choices to be used in the design of bioactive compounds.

The search for cavities using the protease 3D structure PDB code 5R81[46] resulted in the prediction of a less druggable model without the presence of a ligand, and also it was 6for cavities without and with ligand were the same. This behavior was the same as that observed with the use of model PDB 5R82 and the ligand Z219104216.[47] Another model PDB, code 5R84, also presents only the chain A in its structure.[48] It was applied to the study of a cavity search

Table 2. Results of cavity prediction and druggability for protein 3D models from SARS-CoV-2.

Model Protein	Model Cavity	Pred. Max pkd	Pred. Avg pkd	DrugScore	Druggability
5R81*	1	11.90	6.70	−65.00	Less
5R82*	1	10.98	6.38	−152.00	Less
5R84	1	10.02	6.05	−77.00	Less
6LXT	1	10.88	6.96	125.00	Less
	2	10.78	6.31	261.00	Less
	3	7.75	5.28	240.00	Less
6W4B	1	10.88	6.35	1075.00	Yes
	2	9.74	5.96	151.00	Less
	3	5.62	5.63	23.00	Less
6Y84	1	10.72	6.95	−31.00	Less
	2	11.57	6.58	−124.00	Less
	3	11.09	6.42	−97.00	Less
6LU7	1	10.78	6.31	−152.00	Less
6W63*	1	11.26	6.99	199.00	Less
6VWW	1	5.23	6.59	9702.00	Yes
	2	11.33	6.99	−9.00	Less
	3	12.00	6.73	73.00	Less
	4	10.56	6.24	−59.00	Less
	5**	10.66	4.68	−170.00	Less
	6**	10.56	6.24	−424.00	Less
6W01	1	5.59	6.62	9190.00	Yes
	2	4.05	6.55	434.00	Less
	3	11.35	6.99	−284.00	Less
	4	11.83	6.67	−128.00	Less
	5	10.64	6.27	−64.00	Less
	6	9.60	5.91	17.00	Less
	7	8.33	5.65	14.00	Less
6W02	1	9.4	6.87	399.00	Less
	2	11.18	6.45	577.00	Less
	3*	10.35	6.17	588.00	Less
6M3M	1	10.63	6.95	6144.00	Yes
	2	10.64	6.95	−73.00	Less
6VYO	1	6.27	6.66	2526.00	Yes
	2	7.33	6.73	4017.00	Yes
	3	10.17	6.92	1846.00	Yes
	4*	11.51	6.94	328.00	Less
	5*	8.66	6.82	1305.00	Less
	6*	10.38	6.18	116.00	Less

*Cavity in protein 3D models that showed same value isolated and complexed with ligand.**Cavity in protein using chain only A.

that resulted in the prediction of a molecular site considered less druggable, with a drugscore value of −77.00.

The analysis of 3D protease model PDB code 6Y84 without any ligand complexed showed 3 cavities with potential sites of interaction.[49] The results for these cavities were considered less druggable, because these have negative drugscore values. Considering all protease 3D structures evaluated, the 6W63 was suggested to be the best choice to be applied in drug design studies, because it presented higher values of drugscore or this protein showed positive values in less druggable compared to other models studied.

3.2.3 Spike Glycoprotein

Spike proteins are highly glycosylated transmembrane proteins that are grouped into trimers on the surface of the virion which results in a corona-like aspect, "corona".[50] The SARS-CoV-2 protein has approximately 1288 amino acid residues and three chains: A, B, and C. The 3D model of this protein was obtained via Cryo-EM and deposited in the PDB database under the code 6VSB.[51] The search for cavities in this structure, complete with the three chains or even with an isolated chain, did not find a cavity or binding site considered druggable. In the presence of the enzyme complexed ligand, the search for binding sites did not result in the determination of cavities considered viable. This protein, however, is promising for further studies aimed at the development of potential inhibitors.

Table 3. Amino acid residues from druggable cavities according to PDB 3D structure from SARS-CoV-2.

PDB Code	Amino Acid Residues
6VWW	MET:1:A, SER:2:A, LEU:3:A, GLU:4:A, VAL:6:A, ILE:27:A, ASN:29:A, ASN:30:A, THR:31:A, GLU:45:A, ASN:46:A, LYS:47:A, THR:48:A, THR:49:A, LEU:50:A, PRO:51:A, VAL:52:A, ASN:53:A, VAL:54:A, PHE:56:A, GLU:57:A, LEU:58:A, LYS:61:A, VAL:70:A, LYS:71:A, LEU:73:A, ASN:74:A, ASN:75:A, LEU:76:A, GLY:77:A, VAL:78:A, ASP:79:A, ILE:80:A, ASP:88:A, TYR:89:A, LYS:90:A, ARG:91:A, ASP:92:A, ALA:93:A, PRO:94:A, ALA:95:A, HIS:96:A, ILE:97:A, SER:98:A, THR:99:A, ILE:100:A, GLY:101:A, VAL:102:A, CYS:103:A, SER:104:A, MET:105:A, THR:106:A, ASP:107:A, ILE:108:A, ALA:109:A, LYS:110:A, LYS:111:A, THR:113:A, GLU:114:A, THR:115:A, ILE:116:A, CYS:117:A, ALA:118:A, PRO:119:A, LEU:120:A, THR:121:A, ASN:140:A, LYS:181:A, ASP:268:A, PHE:269:A, ILE:270:A, PRO:271:A, MET:272:A, ASP:273:A, SER:274:A, LYS:277:A, THR:326:A, GLN:347:A, MET:1:B, SER:2:B, LEU:3:B, ILE:27:B, ILE:28:B, ASN:29:B, ASN:30:B, THR:31:B, GLU:45:B, ASN:46:B, LYS:47:B, THR:48:B, THR:49:B, LEU:50:B, PRO:51:B, VAL:52:B, ASN:53:B, VAL:54:B, ALA:55:B, GLU:57:B, LEU:58:B, VAL:70:B, LYS:71:B, LEU:73:B, ASN:74:B, ASN:75:B, LEU:76:B, GLY:77:B, VAL:78:B, ASP:79:B, ILE:80:B, ASP:88:B, TYR:89:B, LYS:90:B, ARG:91:B, ASP:92:B, ALA:93:B, PRO:94:B, ALA:95:B, HIS:96:B, ILE:97:B, SER:98:B, THR:99:B, ILE:100:B, GLY:101:B, VAL:102:B, CYS:103:B, SER:104:B, MET:105:B, THR:106:B, ASP:107:B, ILE:108:B, ALA:109:B, LYS:110:B, LYS:111:B, GLU:114:B, THR:115:B, ILE:116:B, CYS:117:B, ALA:118:B, PRO:119:B, LEU:120:B, THR:121:B, ASN:140:B, GLY:141:B, LYS:181:B, LYS:182:B, VAL:183:B, ASP:184:B, GLU:267:B, ASP:268:B, PHE:269:B, ILE:270:B, PRO:271:B, MET:272:B, ASP:273:B, SER:274:B, LYS:277:B, ASN:278:B, THR:326:B, GLN:347:B
6W4B	LEU:46:A, CYS:74:A, ARG:75:A, PHE:76:A, VAL:77:A, LYS:87:A, TYR:88:A, LEU:89:A, PHE:91:A, ASN:97:A, ARG:100:A, GLY:101:A, VAL:103:A, LEU:104:A, GLY:105:A, SER:106:A, LEU:107:A, ALA:108:A, ALA:109:A, VAL:111:A, LEU:113:A, ASN:3:B, GLU:4:B, LEU:5:B, SER:6:B, PRO:7:B, VAL:8:B, ALA:9:B, LEU:10:B, ASN:34:B, THR:35:B, THR:36:B, PHE:41:B, LEU:43:B, ASN:96:B, LEU:98:B, ASN:99:B, MET:102:B
6W01	ALA:0:A, MET:1:A, SER:2:A, LEU:3:A, ILE:27:A, ILE:28:A, ASN:29:A, ASN:30:A, THR:31:A, GLU:45:A, ASN:46:A, LYS:47:A, THR:48:A, THR:49:A, LEU:50:A, PRO:51:A, VAL:52:A, ASN:53:A, VAL:54:A, ALA:55:A, GLU:57:A, LEU:58:A, VAL:70:A, LYS:71:A, LEU:73:A, ASN:74:A, ASN:75:A, LEU:76:A, GLY:77:A, VAL:78:A, ASP:79:A, ILE:80:A, ASP:88:A, TYR:89:A, LYS:90:A, ARG:91:A, ASP:92:A, ALA:93:A, PRO:94:A, ALA:95:A, HIS:96:A, ILE:97:A, SER:98:A, THR:99:A, ILE:100:A, GLY:101:A, VAL:102:A, CYS:103:A, SER:104:A, MET:105:A, THR:106:A, ASP:107:A, ILE:108:A, ALA:109:A, LYS:110:A, LYS:111:A, GLU:114:A, THR:115:A, ILE:116:A, CYS:117:A, ALA:118:A, PRO:119:A, LEU:120:A, THR:121:A, ASN:140:A, ASP:268:A, PHE:269:A, ILE:270:A, PRO:271:A, MET:272:A, ASP:273:A, SER:274:A, LYS:277:A, THR:326:A, LEU:346:A, ALA:0:B, MET:1:B, SER:2:B, LEU:3:B, GLU:4:B, VAL:6:B, ILE:27:B, ASN:29:B, ASN:30:B, THR:31:B, GLU:45:B, ASN:46:B, LYS:47:B, THR:48:B, THR:49:B, LEU:50:B, PRO:51:B, VAL:52:B, ASN:53:B, VAL:54:B, GLU:57:B, LEU:58:B, VAL:70:B, LEU:73:B, ASN:74:B, ASN:75:B, LEU:76:B, GLY:77:B, VAL:78:B, ASP:79:B, ILE:80:B, ASP:88:B, LYS:90:B, ARG:91:B, ASP:92:B, ALA:93:B, PRO:94:B, ALA:95:B, HIS:96:B, ILE:97:B, SER:98:B, THR:99:B, GLY:101:B, VAL:102:B, CYS:103:B, SER:104:B, MET:105:B, THR:106:B, ASP:107:B, ILE:108:B, ALA:109:B, LYS:110:B, LYS:111:B, GLU:114:B, THR:115:B, ILE:116:B, CYS:117:B, ALA:118:B, PRO:119:B, LEU:120:B, THR:121:B, ASN:140:B, LYS:181:B, ASP:268:B, PHE:269:B, ILE:270:B, PRO:271:B, MET:272:B, ASP:273:B
6W63	GLY 23, THR 24, THR 25, THR 26, LEU 27, ASN 28, HIS 41, VAL 42, ILE 43, CYS 44, THR 45, SER 46, GLU 47, ASP 48, MET 49, LEU 50, PRO 52, TYR 54, PHE 140, LEU 141, ASN 142, GLY 143, SER 144, CYS 145, HIS 163, SER 164, MET 165, GLU 166, LEU 167, PRO 168, THR 169, GLY 170, VAL 171, HIS 172, ALA 173, PHE 181, VAL 186, ASP 187, ARG 188, GLN 189, THR 190, ALA 191 and GLN192
6VY0	1: ALA:152:A, ALA:155:A, THR:49:B, ALA:50:B, SER:51:B, TRP:52:B, PHE:53:B, THR:54:B, ALA:55:B, LEU:56:B, THR:57:B, GLN:58:B, HIS:59:B, ARG:88:B, ALA:90:B, ARG:92:B, LEU:104:B, SER:105:B, PRO:106:B, ARG:107:B, TYR:109:B, TYR:111:B, PRO:117:B, ARG:149:B, ASN:150:B, PRO:151:B, ALA:152:B, ASN:153:B, ASN:154:B, ALA:155:B, ALA:156:B, ILE:157:B, VAL:158:B, LEU:159:B, GLN:160:B, LEU:161:B, THR:165:B, THR:166:B, LEU:167:B, PHE:171:B, TYR:172:B, ALA:173:B, TRP:52:C, PHE:53:C, THR:54:C, PRO:73:C, ILE:74:C, ASN:75:C, THR:76:C, ASN:77:C, SER:78:C, ASP:82:C, TYR:112:C, ASP:144:C, HIS:145:C, ILE:146:C, GLY:147:C, THR:148:C, ARG:149:C, ASN:150:C, PRO:151:C, ALA:152:C, ASN:153:C, ASN:154:C, ALA:155:C, ALA:156:C, ILE:157:C, VAL:158:C, LEU:159:C, GLN:160:C, LEU:161:C, ALA:173:C, TRP:52:D, THR:76:D, ASN:77:D, ARG:149:D, ASN:150:D, PRO:151:D, ALA:152:D, ASN:153:D, ASN:154:D, ALA:155:D, ALA:156:D, ILE:157:D, VAL:158:D 2: ALA:50:A, TRP:52:A, PHE:53:A, THR:54:A, ALA:55:A, PRO:73:A, ILE:74:A, ASN:75:A, THR:76:A, ASN:77:A, SER:78:A, ASP:82:A, TYR:112:A, THR:115:A, LYS:143:A, ASP:144:A, HIS:145:A, ILE:146:A, GLY:147:A, THR:148:A, ARG:149:A, ASN:150:A, PRO:151:A, ALA:152:A, ASN:153:A, ASN:154:A, ALA:155:A, ALA:156:A, ILE:157:A, VAL:158:A, LEU:159:A, GLN:160:A, LEU:161:A, ALA:173:A, TRP:52:B, PHE:53:B, THR:54:B, ILE:74:B, ASN:75:B, THR:76:B, ASN:77:B, SER:78:B, ARG:149:B, ASN:150:B, PRO:151:B, ALA:152:B, ASN:153:B, ASN:154:B, ALA:155:B, ALA:156:B, ILE:157:B, VAL:158:B, LEU:159:B, GLN:160:B, PRO:151:C, ALA:152:C, ASN:153:C, ASN:154:C, ALA:155:C, ALA:156:C, GLN:160:C, THR:49:D, ALA:50:D, SER:51:D, TRP:52:D, PHE:53:D, THR:54:D, ALA:55:D, LEU:56:D, THR:57:D, GLN:58:D, HIS:59:D, ARG:88:D, ALA:90:D, THR:91:D, ARG:92:D, ARG:93:D, ILE:94:D, ARG:95:D, GLY:96:D, LYS:102:D, ASP:103:D, LEU:104:D, SER:105:D, PRO:106:D, ARG:107:D, TYR:109:D, TYR:111:D, PRO:117:D, ARG:149:D, ASN:150:D, PRO:151:D, ALA:152:D, ASN:153:D, ASN:154:D, ALA:155:D, ALA:156:D, ILE:157:D, VAL:158:D, LEU:159:D, GLN:160:D, LEU:161:D, PRO:162:D, THR:165:D, THR:166:D, LEU:167:D, PHE:171:D, TYR:172:D, ALA:173:D 3: ALA:50:A, SER:51:A, TRP:52:A, PHE:53:A, THR:54:A, ALA:55:A, LEU:56:A, THR:57:A, HIS:59:A, PRO:73:A, ILE:74:A, ASN:75:A, THR:76:A, ARG:88:A, ARG:92:A, LEU:104:A, SER:105:A, ARG:107:A, TYR:109:A, TYR:111:A, PRO:117:A, ARG:149:A, ASN:150:A, PRO:151:A, ALA:152:A, ASN:153:A, ASN:154:A, ALA:155:A, ALA:156:A, ILE:157:A, VAL:158:A, LEU:159:A, GLN:160:A, LEU:161:A, TYR:172:A, ALA:173:A, THR:49:B, TRP:52:B, PHE:53:B, THR:54:B, PRO:73:B, ILE:74:B, ASN:75:B, THR:76:B, ASN:77:B, SER:78:B, SER:79:B, ASP:82:B, TYR:112:B, LYS:143:B, ASP:144:B, HIS:145:B, ILE:146:B, GLY:147:B, THR:148:B, ARG:149:B, ASN:150:B, PRO:151:B, ALA:152:B, ASN:153:B, ASN:154:B, ALA:155:B, ALA:156:B, ILE:157:B, VAL:158:B, LEU:159:B, GLN:160:B, LEU:161:B, THR:54:D, VAL:158:D, GLN:160:D, ALA:173:D 4: ALA:50:A, TRP:52:A, PHE:53:A, PRO:73:A, ILE:74:A, ASN:75:A, THR:76:A, ASN:77:A, SER:78:A, ASP:82:A, TYR:112:A, THR:115:A, LYS:143:A, ASP:144:A, HIS:145:A, ILE:146:A, GLY:147:A, THR:148:A, ARG:149:A, ASN:150:A, PRO:151:A, ALA:152:A, ASN:153:A,

Table 3. continued

PDB Code	Amino Acid Residues
	ASN:154:A, ALA:155:A, ALA:156:A, ILE:157:A, VAL:158:A, LEU:159:A, GLN:160:A, LEU:161:A, ALA:152:B, ALA:155:B, THR:54:D, ALA:55:D, LEU:56:D, THR:57:D, GLN:58:D, HIS:59:D, ARG:92:D, ARG:93:D, ILE:94:D, ARG:95:D, GLY:96:D, LYS:102:D, ASP:103:D, LEU:104:D, SER:105:D, PRO:106:D, ARG:107:D, TYR:109:D, VAL:158:D, GLN:160:D, LEU:167:D, TYR:172:D, ALA:173:D 5: THR:49:B, ALA:50:B, SER:51:B, TRP:52:B, PHE:53:B, THR:54:B, ALA:55:B, LEU:56:B, THR:57:B, GLN:58:B, HIS:59:B, ARG:88:B, ALA:90:B, ARG:92:B, LEU:104:B, SER:105:B, PRO:106:B, ARG:107:B, TYR:109:B, TYR:111:B, ARG:149:B, ASN:150:B, PRO:151:B, ALA:152:B, ASN:154:B, ALA:155:B, ALA:156:B, ILE:157:B, VAL:158:B, LEU:159:B, GLN:160:B, LEU:161:B, LEU:167:B, TYR:172:B, ALA:173:B, TRP:52:C, PHE:53:C, PRO:73:C, ILE:74:C, ASN:75:C, THR:76:C, ASN:77:C, SER:78:C, ASP:82:C, TYR:112:C, ASP:144:C, HIS:145:C, ILE:146:C, GLY:147:C, THR:148:C, ARG:149:C, ASN:150:C, PRO:151:C, ALA:152:C, ASN:153:C, ASN:154:C, ALA:155:C, ALA:156:C, ILE:157:C, VAL:158:C, LEU:159:C, GLN:160:C, ALA:152:D 6: THR:49:C, ALA:50:C, SER:51:C, TRP:52:C, PHE:53:C, THR:54:C, ALA:55:C, LEU:56:C, THR:57:C, HIS:59:C, ARG:88:C, ALA:90:C, ARG:92:C, ILE:94:C, LEU:104:C, SER:105:C, ARG:107:C, TYR:109:C, TYR:111:C, ARG:149:C, PRO:151:C, ASN:154:C, ALA:155:C, ALA:156:C, ILE:157:C, VAL:158:C, LEU:159:C, TYR:172:C, THR:49:D, ALA:50:D, TRP:52:D, PHE:53:D, ASN:75:D, THR:76:D, ASN:77:D, SER:78:D, SER:79:D, ASP:82:D, TYR:112:D, THR:115:D, LYS:143:D, ASP:144:D, HIS:145:D, ILE:146:D, GLY:147:D, THR:148:D, ARG:149:D, ASN:150:D, PRO:151:D, ALA:152:D, ASN:153:D, ASN:154:D, ALA:155:D, ALA:156:D, ILE:157:D, VAL:158:D

3.2.4 Endoribonuclease

This protein is responsible for lysing virus RNA into smaller portions. In the case of coronavirus, it plays an important role in evading the host's innate immune response. The 3D structural model represented by the PDB code 6VWW refers to the NSP15 endoribonuclease,[52] and it was used to search for likely sites of interaction with inhibitory ligands. This 3D protein model showed four potential binding sites; three of these are less druggable. One of these models showed a positive drugscore value of 73.00, and it can be used in studies of the interaction between bioactive compounds and the binding site from a protein biological target. Studies using the citrate sites of complex on protein and the chain A allowed the prediction of three less druggable models, all of them with negative values for drugscore.

The search for cavities in another 3D model of NSP15 endoribonuclease, PDB code 6W01,[53] resulted in the prediction of eight molecular sites. One was druggable and seven others were classified as less druggable. The druggability cavity model showed a high positive drugscore value of 9190.00, and it can be used in studies of the interaction between bioactive compounds and the molecular site. Due to the greater number of sites considered viable, this protein and its 3D models are among the best options to be used in drug design and development studies for the treatment of COVID-19. The drug baloxavir marboxil used for the treatment of influenza showed inhibition of the viral endonuclease enzyme as the mechanism of action. Li and De Clercq comment that this drug was submitted to clinical studies in China.[39] Due to these findings, this molecule is able to be included in assays for prediction of interactions with cavities predicted from both proteins.

3.2.5 Other Proteins

The 3D models of S2 subunit fusion proteins in the nucleus and the HR2 domain of the S2 subunit were subjected to cavity search analysis. These proteins mediate the fusion and entry of some viruses into the human cell.[54] Therefore, the inhibition of these proteins may be very important in preventing the spread of the infection in human cells. The S2 subunit model containing three chains, A, B and C, PDB code 6LXT,[55] was submitted to cavity search, and this resulted in the prediction of three molecular sites considered less druggable, all with positive score values, 125.00, 261.00, 240.00. The protein HR2 domain of the S2 subunit, code PDB code 6LVN,[56] was also evaluated, and the results of these calculations showed no viable cavities; all of them were considered undruggable. Considering both 3D structures linked to the S2 subunit of SARS-CoV-2, the model 6XLT showed good results and it is suggested to be used in drug design.

Another 3D structure of SARS-CoV-2, the protein N-terminal RNA binding domain from nucleocapsid with four chains A, B, C, and D, PDB code 6M3M,[57] was used in a cavity search. The results showed the prediction of two cavities. The first is druggable with value to Pred. Max pkd of 10.63 and DrugScore 6144.00, and the second cavity is less druggable. The localization of cavities, however, is in a molecular space out of a protein model which characterizes the generation of wrong spatial coordinates and false results. No information about amino acid residues were predicted and these results were not considered. This protein should be used with care before being used in drug design studies.

One more 3D structure observed in the PDB database was 6W02.[58] It refers to the ADP ribose phosphatase NSP3, which was subjected to the search for potential cavities that may be suggested targets of bioactive compounds. The results obtained allowed the prediction of three cavities considered less druggable, but all with high positive values

for drugscore, 599.00, 577.00, and 588.00, respectively. When evaluated in the presence of complexed ligand, a less druggable cavity was found with same values obtained by the third cavity without the presence of ligand. This protein showed an interesting target to be submitted to the search for antiviral inhibitors. The 3D model of RNA binding domain of nucleocapsid protein, PDB code 6VYO,[59] showed three druggable cavities with high positive values for drugscore, 2526.00, 4017.00, and 4017.00 to cavities 1–3. These results indicated this protein as a potential biological target to new antiviral agents.

The study of cavities allowed the prediction of eight druggable cavity sites distributed one each for 6W4B, 6VWW, 6W01, 6M3M and four for 6VYO structures. All cavities are shown in Figure 3 (number 1 is druggable) and

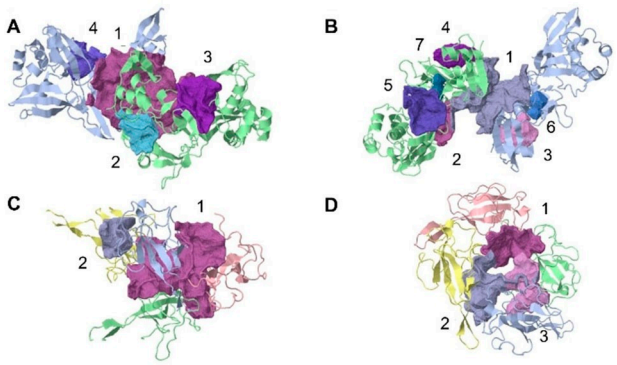

Figure 3. Molecular model 3D of druggable cavities for (A) 6VWW (1–4), (B) 6W01 (1–7), (C) 6M3M (1–2), (D) 6VYO (1–3) in spatial regions using CavityPlus Software.

table 2. The higher drugscore values were determined for 6VWW and 6W01, both are relative to endoribonuclease protein.

CavPharmer tool was applied to a druggable cavity from 6VWW 3D protein, and this allowed the determination of three positive electrostatic points, five negative electrostatic centers, sixteen H-bond acceptor centers and roots, thirty-one H-bond donor centers and roots, and thirty-four hydrophobic centers. These characteristics are important for understanding the bioactive compounds that will interact with this protein model. According the CorrSite, none of the studies showed a Z-score higher than 0.5, which indicates that this cavity is not associated with an allosteric site. No covalent cysteine was determined using the CovCys tool. These results may suggest a better alternative among those studied here to be used as a biological target in studies aiming to develop an antiviral against the SARS-CoV-2.

3.3 Molecular Docking

Molecular docking studies were performed with the best model of protease from SARS-CoV-2 determined by cavities studies, PDB code 6W63 cavity, which showed the highest score among all studied. The protease inhibitors ritonavir and lopiravir that are being assayed against the virus were used in these studies. The lower energy conformers for both drugs were used as individual poses in a docking procedure aimed at evaluating their interactions with a potential active site of the protein.

A model of molecular docking studies of antiretrovirals and interactions with the main protease is demonstrated in Figure 4. This can be used to understand the structural

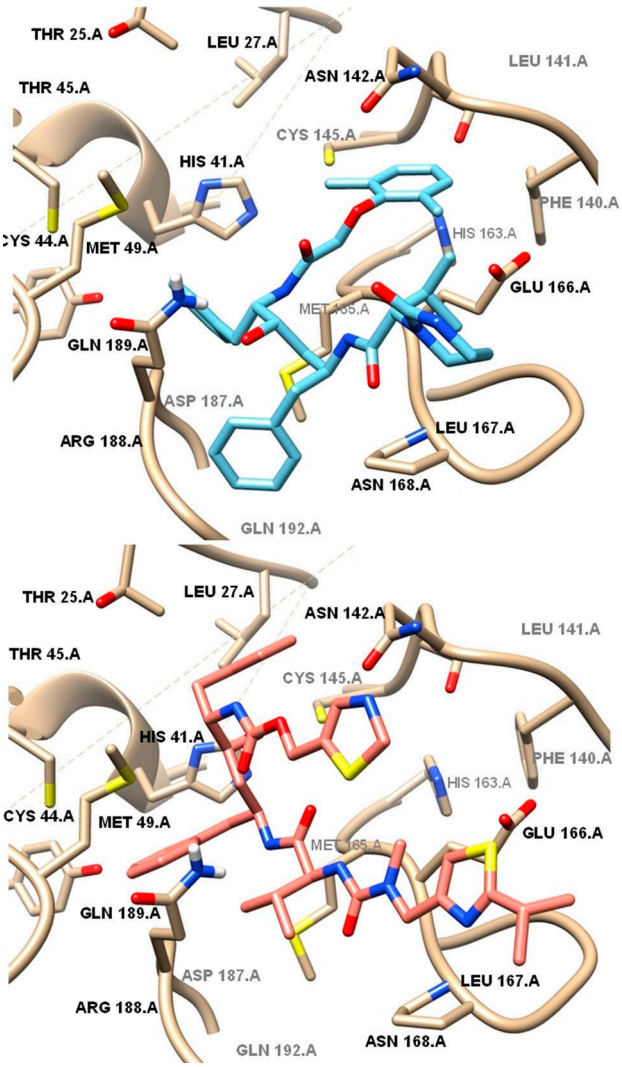

Figure 4. Pose binding mode of ritonavir (A) and lopinavir (B) at active site of main protease of SARS-CoV-2 (PDB code 6W63)[40] using iGemdock 2.1 docking software. Graphic visualization obtained using Chimera (v.1.10.1).

pose affinity with the protein's active site and the predicted cavity. All molecular interaction data are shown in Tables 4 and 5. The order of interaction was ritonavir, which showed less interaction energy (−118.8 Kcal mol^{-1}) compared to lopinavir (−108.3 Kcal mol^{-1}). These results indicate also that ritonavir shows a better fit with the active site in this protease model, and these are in agreement with the findings generated using two antiretroviral drugs and a protease generated by molecular homology.[22] The main interactions generated by this model are shown in Table 5, where the main pose of the two compounds is located in the molecular interaction region of compound X77, co-crystallographed with this protein.

Table 4. Results and the main interactions of the van der Waals type (VDW), H bond, and electrostatic (in Kcal mol^{-1}) coupling with the protease (PDB code 6W63) using the IGemdock 2.1 software.

Compounds	Affinity Energy	VDW	H-bond	Electrostatic
Ritonavir	−118.8	−110.8	−7.9	0.0
Lopinavir	−108.3	−104.8	−3.5	0.0

In this case, the hydrogen bonding interactions occur mainly with the GLU 166 and GLN 189 residues. The predicted van der Waals interactions are observed with the amino acid residues HIS 41, MET 49, ASN 142, MET 165, GLU 166, LEU 167, PRO 168, ASP 187, ARG 188, GLN 189 and GLN192. The amino acid residues are the in the set of set of residues of the results generated by molecular docking and available in the literature.[24,60] Comparing these amino acids with those described in the cavity search results, it is observed that all are inserted in the set of residues listed in the protease cavity. There are forty-three residues in predicted cavity and some of them such as CYS 44, THR 45, PHE 140 and LEU 141 are described in literature as important to result in biological interaction.[60] The lack of interaction with this molecular region may be de cause of lower activity of both antiviral. These data support the hypothesis that the cavity predicted in the 6W63 protease model can be used as a molecular target for the development of compounds that may inhibit this protein, since it showed the best results of druggability among the other protease 3D structures analyzed. However, some amino acids from the predicted cavity considered less druggable did not show interactions with compounds, which may interfere in total protein inhibition. Protease inhibitor drugs are being recommended in some countries for use in severe cases of COVID-19.[61] Nevertheless, their effectiveness has been questioned by researchers,[38,62] based on results that indicate failure in the treatment of studied patients, and the anti-HIV agents were developed to inhibit the aspartic proteases and not cysteine like proteases. However, maybe these compounds don not need to completely fill the spatial regions of the cavity to cause inhibition of this protein. The SARS-CoV-2 protease is an important target for the development of candidate compounds for therapeutic antiviral agents and it should continue to be used in the search for compounds with safe and effective antiviral action.

Another docking study was performed using the replicase protein PDB code 6W4B and drugs such as GS-441524, a nucleoside derivative that is a metabolite active of remdesivir,[34] and favipiravir[33] inhibitors of this enzyme from other viruses. However, the results of docking showed that both chemical structures' interactions with 3D replicase were in a spatial region distinct from the predicted cavity, and also they interact in different locals in this protein. These evaluations may indicate that this protein may not be the target for these drugs.

A model of endoribonuclease PDB code 6VWW[52] was used in docking of the antiviral baloxavir marboxyl aiming to determine characteristics concerning its interaction with this target.[63] The results showed −78.6 Kcal mol^{-1} of energy of pose interaction. Amino acid residues involved in this model were TPR-59, ARG-62, TYR-89, PHE-44, LYS-47 and TRP-87. Only the residues TYR-89, LYS-47 and ASP-92 are in agreement with the residues found in the druggability

Table 5. Central pharmacological interactions (VDW, H-bond, and electrostatic in Kcal mol^{-1}) of compounds and main residues involved in the binding site of protease.

Amino acid Residues	Ritonavir		Lopinavir	
	VDW	H-bond	VDW	H-bond
HIS 41	−14.9	0.0	−3.6	0.0
MET 49	−1.8	0.0	−5.8	0.0
ASN 142	−3.4	0.0	−11.0	0.0
MET 165	−8.4	0.0	−14.3	0.0
GLU 166	−15.7	−3.5	−7.8	0.0
LEU 167	−6.4	0.0	−5.4	0.0
PRO 168	−12.9	0.0	−9.0	0.0
ASP 187	−2.1	0.0	−4.1	0.0
ARG 188	−7.5	0.0	−9.0	0.0
GLN 189	−14.2	0.0	−8.9	−3.5
GLN 192	−0.9	0.0	−6.6	0.0

cavity structure from the 6VWW 3D structure. The interaction of this drug with endoribonuclease needs further studies aimed at determining whether baloxavir marboxyl may be suggested for inclusion in antiviral assays.

4 Conclusions

In this work, some highlights about SARS-CoV-2 3D protein models were verified. Thirteen 3D proteins were evaluated according their potential cavities that may be used in drug design studies. Among these options, the cavity search allowed the identification of eight potential druggable cavity sites in 3D model structures, such as PDB codes 6W4B, 6VWW, 6W01, 6M3M, and 6VYO. These results suggest that these cavities are the best alternatives for molecular targets to be used in studies of new antiviral compounds. Other thirty predicted pocket were considered less druggable, and these may be also used in drug design studies.

The best cavity model of the protease 3D structure, predicted as less druggable, was used in molecular docking studies. The results determined theoric interactions of the amino acid residues from this protein and the antiviral drugs lopinavir and ritonavir. These results may assist the use of 3D protein models in drug design studies aimed at developing drugs against the COVID-19 pandemic.

Conflict of Interest

None declared.

Acknowledgements

The authors thanks to CAPES (DS), FAPERGS (Number 19/2551-0001784-7), and PDA-UNIPAMPA for financial support.

References

[1] J. Cui, F. Li, Z. L. Shi Origin, *Nat. Rev. Microbiol.* **2019**, *17*, 181–192. DOI: 10.1038/s41579-018-0118-9.
[2] A. R. Fehr, S. Perlman, *Methods Mol. Biol.* **2015**, *1282*, 1–23.
[3] S. R. Weiss, J. L. Leibowitz, *Adv. Virus Res.* **2011**, *81*, 85–164. DOI: 10.1016/B978-0-12-385885-6-00009-2.
[4] S. Su, G. Wong, W. Shi, J. Liu, A. C. K. Lai, J. Zhou, W. Liu, Y. By, J. F. Gao, *Trends Microbiol.* **2016**, *24*, 490–502.
[5] A. M. Zaki, S. van Boheemen, T. M. Bestebroer, A. D. Osterhaus, R. A Fouchie, *N. Engl. J. Med.* **2012**, *367*,1814–1820. DOI: 10.1056/NEJMoa1211721.
[6] N. S. Zhong, B. J. Zheng, Y. M. Li, Z. H. X. Poon, K. H. Chan, P. H. Li, S. Y. Tan, Q. Chang, J. P. Xie, X. Q. Liu, J. Xu, D. X. Li, K. Y. Yuen, G. Y. Peiris, *Lancet* **2003**, *362*, 1353-1358. DOI: 10.1016/s0140-6736(03)14630-2.
[7] T. G. Ksiazek, D. Erdman, C. S. Goldsmith, S. R. Zaki, T. Peret, S. Emery, S. Tong, C. Urbani, J. A. Comer, W. Lim, P. E. Rollin, S. F. Dowell, A.-E. Ling, C. D. Humphrey, W.-J. Shieh, J. Guarner, C. D. Paddock, et al., *N. Engl. J. Med.* **2003**, *348*, 1953–1966. DOI: 10.1056/NEJMoa030781.
[8] C. Drosten, S. Günther, W. Preiser, S. van der Werf, H.-R. Brodt, S. Becker, H. Rabenau, M. Panning, L. Kolesnikova, R. A. M. Fouchier, A. Berger, A.-M. Burguière, J. Cinatl, M. Eickmann, N. Escriou, K. Grywna, S. Kramme, et al., *N. Engl. J. Med.* **2003**, *348*, 1967–1976. DOI: 10.1056/NEJMoa030747.
[9] D. Normile, *Science* **2020**, *367*, 6485. DOI:10.1126/science.aba7672.
[10] N. Zhu, D. Zhang, W. Wang, X. Li, B. Yang, J. Song, X. Zhao, B. Huang, W. Shi, R. Lu, P. Niu, F. Zhan, X. Ma, D. Wang, W. Xu, G. Wu, G. F. Gao, D. Phil, W. Tan, *N. Engl. J. Med.* **2020**, *382*, 8, 727–733.
[11] C. Huang, X. Li, L. Ren, J. Zhao, Y. Hu, L. Zhang, G. Fan, J. Xu, X. Gu, Z. Cheng, T. Yu, J. Xia, Y. Wei, W. Wu, X. Xie, W. Yin, H. Li, M. Liu, Y. Xiao, H. Gao, L. Guo, J. Xie, G. Wang, R. Jiang, Z. Gao, Q. Jin, J. Wang, B. Cao, *Lancet*, **2020**, *395*, 497–506. DOI: 10.1016/S0140-6736(20)30183-5.
[12] World Health Organization. https://www.who.int/dg/speeches/detail/who-director-general-s-opening-remarks-at-the-media-briefing-on-covid-19-11-march-2020. Accessed in March 2020.
[13] D. Wang, C. Hu, F. Zhu, X. Liu, J. Zhang, B. Wang, H. Xiang, Z. Cheng, Y. Xiong, Y. Zhao, Y. R. Li, X. Wang, Z. Peng, *JAMA.* **2020**, *323*, 1061–1069. DOI:10.1001/jama.2020.1585.
[14] G. F. Gao, *Cell* **2018**, *172*, 1157–1159. https://DOI.org/10.1016/j.cell.2018.02.025.
[15] Y. M. Arabi, A. Y. Asiri, A. M. Assiri, H. A. A. Jokhdar, A. Alothman, H. H. Balkhy, S. Al Johani, S. Al Harbi, S. Kojan, M. Al Jeraisy, A. M. Deeb, Z. A. Memish, S. Ghazal, S. Al Faraj, F. Al-Hammed, A. AlSaedi, Y. Mandourah, G. A. Al Mekhalafi, et al., *Trials* **2020**, *21*, 8. DOI: 10.1186/s13063-019-3846-x.
[16] Y. P. Chong, J. Y. Song, Y. B. Seo, J.-P. Choi, H.-S. Shin, *Infect. Chemother.* **2015**, *47*, 212–222. DOI: 10.3947/ic.2015.47.3.312.
[17] V. Nukoolkarn, V. S. Lee, M. Malaisree, O. Aruksakulwong, S. Hannongbua, *J. Theor. Biol.* **2008**, *254*, 861–867. DOI: 10.1016/j.jtbi.2008.07.030.
[18] C. M. Chu, V. C. Chen, I. F. Hung, M. M. Wong, K. H. Chan, R. Y. Kao, L. L. Poon, C. L. Wong, J. S. Peiris, K. Y. Yuen, *Thorax* **2004**, *59*, 252–256. DOI: 10.1136/thorax.2003.012658.
[19] M. A. Martinez, *Antimicrob. Agents Chemother.* **2020**, *337*. DOI:10.1128/AAC.00399.
[20] J. Liu, R. Cao, M. Xu, X. Wang, H. Zhang, H. Hu, Y. Li, Z. Hu, W. Zhong, M. Wang, *Cell Discov.* **2020**, *6*. DOI: 10.1038/s41421-020-0156-0.
[21] RCSB Protein Data Bank.
[22] S. Lin, R. Shen, J. He, S. Li, X. Guo, *bioRxiv* **2020**. DOI: 10.1101/2020.01.31.929695.
[23] L. Zhang, D. Lin, X. Sun, U. Curth, C. Drosten, L. Sauerhering, S. Becker, K. Rox, R. Hilgenfeld, *Science* **2020**. DOI: 10.1126/science.abb3405.
[24] A. T. Ton, F. Gentile, M. Hising, F. Ban, A. Cherkasov, *Mol. Inf.* **2020**, *39*, 2000028.
[25] Y. Xu, S. Wang, Q. Hu, S. Gao, X. Ma, W. Zhang, Y. Shen, F. Chen, L. Lai, J. Pei, *Nucleic Acids Res.* **2018**, *46*, W374–W379. DOI: 0.1093/nar/gky380.
[26] G. M. Morris, R. Huey, W. Lindstrom, M. Sanner, R. K. Belew, D. S. Goodsell, A. J. Olson, *J. Comput. Chem.* **2009**, *16*, 2785–2791.
[27] J. M. Yang, C. C. Chen, *Proteins* **2004**, *55*, 288–304.
[28] X. Liu, B. Zhang, Z. Jin, H. Yang, Z. Rao, *RCSB Protein Data Bank* **2020**, DOI 10.2210/PDB6LU7/pdb.

[29] A. L. Cheng, R. G. Coleman, K. T. Smyth, Q. Cao, P. Soulard, D. R. Caffrey, A. C. Salzberg, E. S. Huang, *Nature* **2007**, *25*, 71–75.
[30] K. Tan, Y. Kim, R. Jedrzejczak, N. Maltseva, M. Endres, K. Michalska, A. Joachimiak, *RCSB Protein Data Bank* **2020**. DOI: 10.2210/pdb6W4B/pdb.
[31] T. K. Warren, R. Jordan, M. K. Lo, A. S. Ray, R. L. Mackman, V. Soloveva, D. Siegel, M. Perron, R. Bannister, H. C. Hui, N. Larson, R. Strickley, J. Wells, K. S. Stuhman, S. A. Van Tonegeren, N. L. Garza, G. Donnely, et al., *Nature* **2016**, *531*, 381–385. DOI: 10.1038/nature17180.
[32] M. L. Agostini, E. L. Andres, A. C. Sims, R. L. Graham, T. P. Sheahan, X. Lu, E. C. Smith, J. B. Case, J. Y. Feng, R. Jordan, A. S. Ray, T. Cihlar, D. Siegel, R. L. Mackman, M. O. Clarke, R. S. Baric, M. R. Denison, *mBio* **2018**, *9*, e00221-18. DOI: 10.1128/mBio.00221-18.
[33] Y. Furuta, K. Takahashi, K. Shiraki, K. Sakamoto, D. F. Smee, D. L. Barnard, B. B. Gowen, J. G. Julander, J. D. Morrey, *Antiviral Res.* **2009**, *82*, 95–102. DOI:10.1016/j.antiviral.2009.02.198.
[34] M. L. Holshue, C. DeBolt, S. Lindquist, K. H. Lofy, J. Wiesman, H. Bruce, C. Spitters, K. Ericson, S. Wilkerson, A. Tural, G. Diaz, A. Cohn, L. Fox, A. Patel, S. I. Gerber, L. Kim, S. Ton, et al., *N. Eng. J. Med.* **2020**, *382*, 929–936. DOI:10.1056/NEJMoa2001191.
[35] E. S. F. Muri, *Quim. Nova* **2014**, *37*, 308–316. DOI: 10.5935/0100-4042.20140052.
[36] G. Leonis, T. Steinbrecher, M. G. Papadopoulos, *J. Chem. Inf. Model.* **2013**, *53*, 2141–2153. DOI: 10.102/ci4002102.
[37] L. Izquierdo, F. Helle, C. François, S. Castelain, G. Duverlie, E. Brochot, *Pharmgenomics Pers. Med.* **2014**, *7*, 241–249. DOI: 10.2147/PGPM.S52715.
[38] B. Cao, Y. Wang, D. Wen, W. Liu, J. Wang, G. Fan, L. Ruan, B. Song, Y. Cai, M. Wei, X. Li, J. Xia, N. Chen, J. Xiang, T. Yu, T. Bai, et al., *N. Engl. J. Med.* **2020**. DOI: 10.1056/NEJMoa2001282.
[39] G. Li, E. De Clercq, *Nat. Rev. Drug Discovery* **2020**, *19*, 149–150. DOI: 10.1038/d41573-020-00016-0.
[40] A. D. Mesecar, *RCSB Protein Data Bank* **2020**. DOI: 10.2210/pdb6W63/pdb.
[41] D. Fearon, A. J. Powell, A. Douangamath, C. D. Owen, C. Wild, T. Krojer, P. Lukacik, C. M. Strain-Damereli, M. A. Walsh, F. von Delft, *RCSB Protein Data Bank* **2020**. DOI: 10.2210/pdb5R80/pdb.
[42] D. Fearon, A. J. Powell, A. Douangamath, C. D. Owen, C. Wild, T. Krojer, P. Lukacik, C. M. Strain-Damereli, M. A. Walsh, F. von Delft, *RCSB Protein Data Bank* **2020**. DOI: 10.2210/pdb5R7Y/pdb.
[43] D. Fearon, A. J. Powell, A. Douangamath, C. D. Owen, C. Wild, T. Krojer, P. Lukacik, C. M. Strain-Damereli, M. A. Walsh, F. von Delft, *RCSB Protein Data Bank* **2020**. DOI: 10.2210/pdb5R7Z/pdb.
[44] D. Fearon, A. J. Powell, A. Douangamath, C. D. Owen, C. Wild, T. Krojer, P. Lukacik, C. M. Strain-Damereli, M. A. Walsh, F. von Delft, *RCSB Protein Data Bank* **2020**. DOI: 10.2210/pdb5R83/pdb.
[45] B. Zhang, Y. Zhao, Z. Jin, X. Liu, H. Yang, Z. Rao, *RCSB Protein Data Bank* **2020**. DOI: 10.2210/pdb6M03/pdb.
[46] D. Fearon, A. J. Powell, A. Douangamath, C. D. Owen, C. Wild, T. Krojer, P. Lukacik, C. M. Strain-Damereli, M. A. Walsh, F. von Delft, *RCSB Protein Data Bank*,**2020**. DOI: 10.2210/pdb5R81/pdb.
[47] D. Fearon, A. J. Powell, A. Douangamath, C. D. Owen, C. Wild, T. Krojer, P. Lukacik, C. M. Strain-Damereli, M. A. Walsh, F. von Delft, *RCSB Protein Data Bank* **2020**. DOI: 10.2210/pdb5R82/pdb.
[48] D. Fearon, A. J. Powell, A. Douangamath, C. D. Owen, C. Wild, T. Krojer, P. Lukacik, C. M. Strain-Damereli, M. A. Walsh, F. von Delf, *RCSB Protein Data Bank* **2020**. DOI: 10.2210/pdb5R84/pdb.
[49] C. D. Owen, P. Lukacik, C. M. Strain-Damerell, A. Douangamath, A. J. Powell, D. Fearon, J. Brandao-Neto, A. D. Crawshaw, D. Aragao, M. Williams, R. Flaig, D. R. Hall, K. E. McAuley, M. Mazzorana, D. I. Stuart, F. von Delft, M. A. Walsh, *RCSB Protein Data Bank* **2020**. DOI: 10.2210/pdb6Y84/pdb.
[50] S. Belouzard, J. K. Millet, B. N. Licitra, G. R. Whittaker, *Viruses* **2012**, *4*, 1011–1033. DOI: 10.3390/v4061011.
[51] D. Wrapp, N. Wang, K. S. Corbett, J. A. Goldsmith, C. Hsieh, O. Abiona, B. S. Graham, J. S. McLellan, *RCSB Protein Data Bank* **2020**. DOI: 10.2210/pdb6VSB/pdb.
[52] Y. Kim, R. Jedrzejczak, N. Maltseve, M. Endres, A. Godzik, K. Michalska, A. Joachimiak, *RCSB Protein Data Bank* **2020**. DOI: 10.2210/pdb6VWW/pdb.
[53] Y. Kim, R. Jedrzejczak, N. Maltseve, M. Endres, A. Godzik, K. Michalska, A. Joachimiak, *RCSB Protein Data Bank* **2020**. DOI: 10.2210/pdb6w01/pdb.
[54] S. Xia, Y. Zhu, M. Liu, Q. Lan, W. Xu, Y. Wu, T. Ying, S. Liu, S. Shi, S. Jiang, L. Lu, *Cell. Mol. Immunol.* **2020**. DOI: 10.1038/s41423-020-0374-2.
[55] Y. Zhu, F. Sun, *RCSB Protein Data Bank* **2020**. DOI: 10.2210/pdb6LXT/pdb.
[56] Y. Zhu, F. Sun, *RCSB Protein Data Bank* **2020**. DOI: 10.2210/pdb6LVN/pdb.
[57] S. Chen, S. Kang, *RCSB Protein Data Bank* **2020**. DOI: 10.2210/pdb6M3M/pdb.
[58] K. Michalska, Y. Kim, R. Jedrzejczak, N. Maltseva, M. Endres, A. Mececar, A. Joachimiak, *RCSB Protein Data Bank* **2020**. DOI: 10.2210/pdb6W02/pdb.
[59] C. Chang, K. Michalska, R. Jedrzejczak, N. Maltseva, M. Endres, A. Godzik, Y. Kim, A. Joanchimiak, *RCSB Protein Data Bank* **2020**. DOI: 10.2210/pdb6VYO/pdb.
[60] M. Macchiagodena, M. Pagliai, P. Procacci, *Chem. Phys. Lett.* **2020**, *750*, 137489. DOI: 10.1016/j.cplett.2020.137489.
[61] E. Teslova, Russia recommends lopinavir/ritonavir against COVID-19. https://www.aa.com.tr/en/health/russia-recommends-lopinavir-ritonavir-against-covid-19/1778844. **2020**. Accessed in March 25.
[62] T. P. Sheahan, A. C. Sims, S. R. Leist, A. Shafer, J. Won, A. J. Brown, S. A. Montgomery, A. Hoog, D. Babusis, M. O. Clarke, J. E. Spahn, L. Bauer, S. Sellers, D. Porter, J. Y. Feng, T. Cihlar, R. Jordan, M. R. Denison, R. S. Baric, *Nat. Commun.* **2020**, *11*, 222–222. DOI: 10.1038/s41467-019-13940-6.
[63] A. J. Eisfeld, G. Neumann, Y. Kamaoka, *Nat. Rev. Microbiol.* **2015**, *13*, 28–41. DOI: 10.1038/nmicro3367.

Received: April 20, 2020
Accepted: August 4, 2020
Published online on October 20, 2020

